IEEE Access
Multidisciplinary | Rapid Review | Open Access Journal

Received July 7, 2020, accepted July 19, 2020, date of publication July 23, 2020, date of current version August 4, 2020.

Digital Object Identifier 10.1109/ACCESS.2020.3011404

Current Distribution and Input Impedance of a VLF Tubular Antenna in a Cold Plasma

LINA HE[1], (Graduate Student Member, IEEE), TONG HE[2], (Member, IEEE), HUI RAN ZENG[1], (Graduate Student Member, IEEE), AND KAI LI[1]

[1]College of Information Science and Electronic Engineering, Zhejiang University, Hangzhou 310027, China
[2]Intelligent Network Research Center, Zhejiang Lab, Hangzhou 311121, China

Corresponding authors: Tong He (tongh@zhejianglab.com) and Kai Li (kaili@zju.edu.cn)

This work was supported in part by the National Natural Science Foundation of China (NSFC) under Grant 61571389 and Grant 61271086.

ABSTRACT As the U.S. and Europe launched the very low frequency (VLF: 3–30 kHz) space-borne transmitting and propagation experiments during the past thirty years, space-borne antennas have been playing a more and more important role in contemporary VLF communication systems, which are very likely to become an indispensable approach for overwater/underwater communication and navigation in the future. In this paper, we propose a semianalytical method for evaluating the current distribution and input impedance of a VLF space-borne tubular antenna. By considering the effects of both the ordinary wave (O-wave) and the extraordinary wave (E-wave) in an anisotropic ionosphere, the analytical expression for the current distribution has a more complicated form and is derived via the method of moments (MoM) and the Gauss-Legendre quadrature (GLQ) algorithm. Computations show that the current distribution and input impedance under anisotropic conditions are very sensitive to parameter changes, but the overall trend for the input impedance will increase with the radius or electrical length of the antenna. Comparisons with linear models and numerical results obtained in FEKO verify the accuracy of this method. From simulations about the effect of the geomagnetic inclination angle to the input impedance, we advise that the parallel case can be preferred as an alternative for the best angle. Once all antenna parameters are determined, there is a possibility to find multiple optimal inclination angles. In addition, qualitative analyses of the impact of environmental changes to the antenna characteristics are also discussed.

INDEX TERMS Anisotropic plasma, current distribution, tubular antenna.

I. INTRODUCTION

It is known that the very low frequency (VLF: 3–30 kHz) electromagnetic waves are widely used in overwater/underwater communication and navigation. However, most of the existing VLF communication systems required huge ground-based transmitting stations, which often covered more than several square kilometers and were very difficult to repair in time once damaged. With the progresses in space technology and the decrease on satellite launching cost, the possibility of establishing a VLF space-borne transmitting system began to enter people's minds, and a feasible scheme was to tether the antenna to a low-earth satellite. Since these satellites usually operate on low-earth orbits (LEO) of 300–400 km, this height is right located in the F_2 layer of the ionosphere, where the ionospheric parameters are relatively stable [1]. For one thing, the ambient plasma near a space-borne antenna has a refractive index of 50–150 at the VLF band [2], thus both the electrical length and radiation efficiency of the antenna can be greatly improved without increasing its geometric size. On the other hand, as the satellites will move around the earth, the propagation distance between the transmitter and the receiver is also significantly shortened, which will further reduce the transmission losses. The above advantages of a VLF space-borne transmitting system may enable it to realize global overwater/underwater communication and navigation without consuming very great power.

Since the 1990s, a few countries including the U.S. and Russia had initiated the investigations on VLF space-borne transmitting and propagation experiments [3]–[7]. In 1992, NASA and the Italian Space Agency (ASI) launched a joint project aiming to deploy a 20 kilometers long conducting tether which connected from a tethered satellite system (TSS) to a space shuttle. The long conducting tether was then regarded as a VLF transmitting antenna. TSS-1R was a reflight of the TSS-1 satellite whose mission was aimed to test the TSS system and examine the

The associate editor coordinating the review of this manuscript and approving it for publication was Debdeep Sarkar.

electromagnetic interaction between the TSS and the ambient space plasma [8]. In addition, many other missions like the imager for magnetopause-to-aurora global exploration (IMAGE) have been developed [9], [10]. Zhangheng-1 or CSES (China Seismo-Electromagnetic Satellite), which is a Chinese research satellite studying the ionospheric precursors of earthquakes, has been successfully launched in 2018. It was a collaboration between the China National Space Administration (CNSA) and the Italian Space Agency (ASI) [11]. In contrast, Russia adopted a large loop antenna as the transmitting device. In 1987, the Soviet Union successfully deployed two loop antennas with a diameter of 20 meters in the ''Progress-28'' space station for transmitting VLF waves [4]. It is worth noting that both the experiments implemented by the U.S. and Russia had proved that VLF electromagnetic signals transmitted from a low-earth satellite could penetrate the ionosphere and propagate to the earth's surface effectively. Theoretical studies on VLF space-borne transmission and propagation were also carried out by researchers during the past thirty years. In 1993, the wave propagation theory for a VLF space-borne linear antenna was initially investigated by Bannister *et al.* [6], where the effect of the earth's magnetic field was only considered on the wave number. In 2001, Nikitin and Swenson [12] calculated the radiation impedance of a short dipole antenna in an anisotropic cold plasma by using a quasi-static method. The current distribution and terminal impedance of a VLF electric dipole antenna in the magnetosphere were then examined by Bell *et al.* [13] in 2006 and by Chevalier *et al.* [14] in 2008, respectively. Since the 2000s, a few Russian scientists such as Zaboronkova, Kudrin, and Chugunov [15]–[18] also conducted extensive research on the current distributions and input impedances of VLF loop and cylindrical antennas in an anisotropic magnetoplasma. In the 2010s, in-depth investigations on the propagation theory for VLF/ELF (extremely low frequency: 3–30 Hz) waves excited by electric/magnetic dipole antennas in an anisotropic ionosphere were carried out by Li *et al.* [19] and Pan and Li [20]. In two recent papers by He *et al.* [21], [22], the current distribution and input impedance of a VLF space-borne linear antenna parallel or at arbitrary orientations to the earth's magnetic field were investigated in detail.

When designing a linear antenna, it would be beneficial to obtain its current distribution and input impedance in order to improve the antenna efficiency. Unfortunately, due to the complex anisotropic properties of the ionosphere in the VLF band, computing the current distribution on a VLF space-borne linear antenna was never an easy job. By considering the anisotropy of the ionosphere caused by the earth's magnetic field, VLF waves produced by space-borne antennas will be separated into two modes, namely, the ordinary wave (O-wave) and the extraordinary wave (E-wave). When the antenna operates at a height of low-earth orbit, its transmitted O-wave is an evanescent wave, while the E-wave is a propagable mode with small attenuation rate. Hence in previous works, contributions from the O-wave were often neglected when computing the far-field. Considering that the current distribution and input impedance are mainly dependent on the fields in the near region (i.e., $k\rho \ll 1$), where the O-wave still has comparable amplitudes with the E-wave [23], both the influences of the O-wave and E-wave should be taken into account when dealing with a VLF space-borne antenna. Moreover, because of the skin effect caused by the alternating currents inside a conductor, the current distribution on a linear antenna will inevitably tend to the surface of the antenna. In this case, the assumptions concerning a long and thin antenna are no longer accurate, instead the model of a tubular antenna assuming the currents aggregating on the antenna surface will be more close to the real situation. In this regard, though there exists a few works focusing on the tubular antenna, it does not receive enough attention it deserves. In 1970, Chang and Wait [24] present a partly numerical method to investigate the input admittance and current distribution of a finite vertical tubular dipole antenna over an infinite dissipative half-space. King et.al [25] and Shen and Wu [26] have dealt with this problem in an isotropic plasma subsequently. When the medium is regarded as an anisotropic one, numerical results based on the Clemmow-Mullaly-Allis diagram were obtained by Bhat [27]. It is a pity that no effort has ever directed toward calculating them analytically. Therefore, as the importance of VLF space-borne transmitting systems will continue growing in the next few decades, the lack of reliable analytical solutions to this problem is the motivation for the present study.

In this paper, we will attempt to propose a new theoretical method for evaluating the current distribution and input impedance of a VLF space-borne tubular antenna. The ambient ionosphere of the antenna is regarded as a homogeneous anisotropic cold plasma, where all the sheath effects and wave-plasma interactions are ignored. The main contribution of this paper is to take into account the skin effect of the current, so that the current should be distributed on the outer surface rather than concentrated on the axis. Consequently, the treatment of a tubular model instead of a purely linear one is desirable. In terms of the physical model, it has a more solid geometric sense. And in terms of the mathematical formula, the kernel function is a triple integral and the current distribution will also differ from our original work in [21]–[23]. Moreover, the effect of the geomagnetic inclination angle to the input impedance of a tubular antenna is also considered in this work. The rest of the paper is organized as follows: the analytical derivation procedures for determining the current distribution and input impedance are provided in Section II. Based on this method, some computations and discussions under different conditions are carried out in Section III. Finally, the paper concludes in Section IV.

II. FORMULATIONS OF THE PROBLEM

A. GEOMETRY AND NOTATIONS OF THE PHYSICAL MODEL

The physical model of the discussed problem is illustrated in Fig. 1. The center-driven antenna is composed of a very thin and highly conducting tube with radius a and length $2h$,

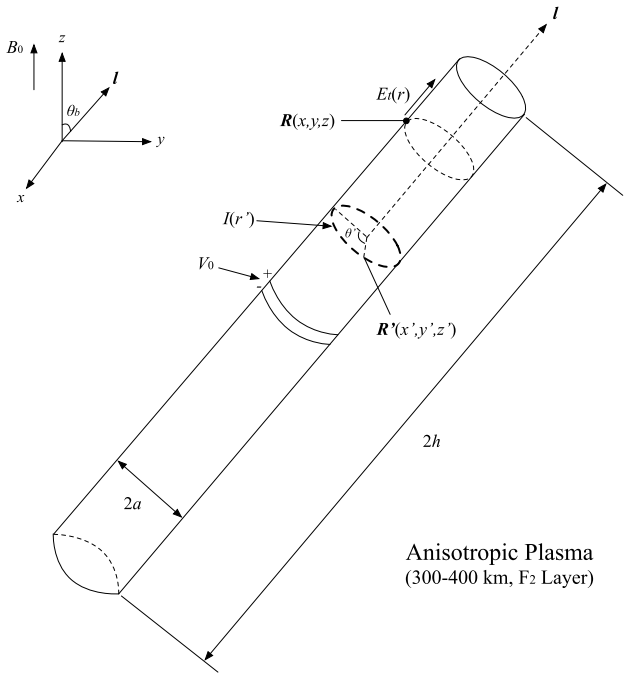

FIGURE 1. Geometry and notations of a VLF space-borne tubular antenna in a homogeneous anisotropic plasma.

where $a \ll h$. The center of the tube is located at the origin of the coordinate system where a drive voltage V_0 is applied to maintain an axial current. Generally, the angle between the tethered antenna and the earth's magnetic field is not constant, but will change with the satellite moving along the orbit. For simplicity, we put the antenna in the $\hat{y}$-$\hat{z}$ plane, and let the geomagnetic field always be oriented along the $\hat{z}$ axis. Then the angle between the directional vector of the antenna $\boldsymbol{l}$ and the $\hat{z}$ axis can be defined as the geomagnetic inclination angle θ_b.

Using a cold plasma treatment, the ambient environment of the antenna is equivalent to a homogeneous anisotropic plasma characterized by the following relative dielectric tensor and permeability [20], [28]

$$\hat{\varepsilon} = \begin{bmatrix} \varepsilon_1 & -i\varepsilon_2 & 0 \\ i\varepsilon_2 & \varepsilon_1 & 0 \\ 0 & 0 & \varepsilon_3 \end{bmatrix} \tag{1}$$

$$\mu_r = 1 \tag{2}$$

where

$$\varepsilon_1 = 1 - \frac{XU}{(U^2 - Y^2)},\ \varepsilon_2 = \frac{XY}{(U^2 - Y^2)},\ \varepsilon_3 = 1 - \frac{X}{U} \tag{3}$$

$$U = 1 + i\frac{\nu}{\omega},\quad X = \frac{\omega_0^2}{\omega^2},\ Y = \frac{\omega_H}{\omega} \tag{4}$$

$$\omega_0^2 = \frac{Ne^2}{\varepsilon_0 m_e},\quad \omega_H = \left|\frac{eB_0}{m_e}\right| \tag{5}$$

In above formulas, ω_0 and ω_H are the plasma frequency and gyro frequency, respectively, and $\omega = 2\pi f$ is the angular operating frequency. B_0 represents the magnitude of the geomagnetic field, and m_e and e denote the mass and charge quantity of an electron, respectively. The electron density and collision frequency for the ionosphere are denoted by N and ν, respectively. Besides, ε_0, μ_0, and $k_0 = \omega\sqrt{\mu_0\varepsilon_0}$ are the permittivity, permeability, and wave number in free space, respectively. In the whole text, the time harmonic factor $\exp(-i\omega t)$ is assumed and suppressed.

With the rotational symmetry satisfied, the axial current should aggregate on the surface of the tube. Thus the total current at r' can be expressed by

$$I(r') = 2\pi a K(r') \tag{6}$$

where $K(r')$ denotes the surface density of the axial current.

It is seen that the distance from a surface current element located by $\boldsymbol{R'}(x', y', z')$ to an observation point located by $\boldsymbol{R}(x, y, z)$ on the surface of the tube is

$$|\boldsymbol{R} - \boldsymbol{R'}| = \sqrt{(x - x')^2 + (y - y')^2 + (z - z')^2} \tag{7}$$

For convenience, we also put $\boldsymbol{R}(x, y, z)$ in the $\hat{y}$-$\hat{z}$ plane and make it above the axis of the antenna. Then the relative coordinate between $\boldsymbol{R}$ and $\boldsymbol{R'}$ can be rewritten as

$$x - x' = -a\sin\theta' = \tilde{x} \tag{8}$$

$$y - y' = (r - r')\sin\theta_b - (1 - \cos\theta')\, a\cos\theta_b = \tilde{y} \tag{9}$$

$$z - z' = (r - r')\cos\theta_b + (1 - \cos\theta')\, a\sin\theta_b = \tilde{z} \tag{10}$$

where $-h \le r, r' \le h$.

Here, θ' represents the angle between the projections of $\boldsymbol{R}$ and $\boldsymbol{R'}$ when they are in a same plane. By using (8)–(10), the relative position between $\boldsymbol{R}$ and $\boldsymbol{R'}$ in cylindrical coordinates can be expressed with $(\tilde{\rho}, \tilde{\varphi}, \tilde{z})$. We have

$$\tilde{\rho} = \sqrt{\tilde{x}^2 + \tilde{y}^2},\qquad \tilde{\varphi} = \tan^{-1}\frac{\tilde{y}}{\tilde{x}} \tag{11}$$

and the longitudinal distance $\tilde{z}$ remains constant.

B. TANGENTIAL COMPONENT OF THE ELECTRIC FIELD AND ITS SATISFIED BOUNDARY CONDITION

According to our previous work [22], the tangential electric field excited by an arbitrarily oriented electric dipole in an infinite homogeneous anisotropic plasma could be expressed in the following form

$$\begin{aligned} &E_t(\rho, \varphi, z) \\ &= \frac{-i\omega\mu_0}{(2\pi)^2}\int_{-\infty}^{\infty}\exp(-ik_z z)dk_z \\ &\quad\times\int_0^{\infty}\left[\frac{\cos^2\theta_b W_1(k_z,\lambda) + \sin^2\theta_b W_2(k_z,\lambda,\varphi)}{B(k_z,\lambda)}J_0(\lambda\rho)\right. \\ &\quad\left.+\frac{\sin^2\theta_b W_3(k_z,\lambda,\varphi) + \sin\theta_b\cos\theta_b W_4(k_z,\lambda,\varphi)}{B(k_z,\lambda)}J_1(\lambda\rho)\right] \\ &\quad\times\lambda d\lambda \end{aligned} \tag{12}$$

where J_0 and J_1 are the zero-order and first-order Bessel functions of the first kind, respectively. In addition, the expressions for $B(k_z, \lambda)$, $W_1(k_z, \lambda)$, $W_2(k_z, \lambda, \varphi)$, $W_3(k_z, \lambda, \varphi)$,

and $W_4(k_z, \lambda, \varphi)$ are given by

$$B(k_z,\lambda) = k_0^6\left[\left(\frac{k_z}{k_0}\right)^4\varepsilon_3 + \left(\frac{\lambda}{k_0}\right)^2\left(\varepsilon_2^2-\varepsilon_1^2-\varepsilon_1\varepsilon_3\right) + \left(\frac{k_z}{k_0}\right)^2\left(\frac{\lambda}{k_0}\right)^2(\varepsilon_1+\varepsilon_3) - 2\left(\frac{k_z}{k_0}\right)^2\varepsilon_1\varepsilon_3 + \varepsilon_3\left(\varepsilon_1^2-\varepsilon_2^2\right) + \left(\frac{\lambda}{k_0}\right)^4\varepsilon_1\right] \tag{13}$$

$$W_1(k_z,\lambda) = \left(k_z^2+\lambda^2\right)k_z^2 - k_0^2\varepsilon_1\left(2k_z^2+\lambda^2\right) + k_0^4\left(\varepsilon_1^2-\varepsilon_2^2\right) \tag{14}$$

$$W_2(k_z,\lambda,\varphi) = k_0^2\left(k_0^2\varepsilon_1\varepsilon_3 - \varepsilon_1\lambda^2 - \varepsilon_3 k_z^2\right) + \left(\frac{\cos 2\varphi+1}{2}\right)\lambda^2\left(k_z^2+\lambda^2-k_0^2\varepsilon_3\right) \tag{15}$$

$$W_3(k_z,\lambda,\varphi) = -\lambda\left(k_z^2+\lambda^2-k_0^2\varepsilon_3\right)\left(\frac{\cos 2\varphi}{\rho}\right) \tag{16}$$

$$W_4(k_z,\lambda,\varphi) = -2ik_z\lambda\left(k_z^2+\lambda^2-k_0^2\varepsilon_1\right)\cos\varphi \tag{17}$$

Considering the relative coordinate between the observation point and the surface current element is $(\tilde{\rho}, \tilde{\varphi}, \tilde{z})$, the tangential component of the total electric field excited on the surface of the tube could be written as

$$E_t(r) = \frac{-i\omega\mu_0}{(2\pi)^2}\int_{-h}^{h}\int_0^{2\pi} G(\tilde{\rho},\tilde{\varphi},\tilde{z})\, I(r')d\theta' dr' \tag{18}$$

where $G(\tilde{\rho}, \tilde{\varphi}, \tilde{z})$ is the kernel function of the antenna. We write

$$G(\tilde{\rho},\tilde{\varphi},\tilde{z}) = \int_{-\infty}^{\infty}\exp(-ik_z\tilde{z})dk_z \times \int_0^{\infty}\left[\frac{\cos^2\theta_b W_1(k_z,\lambda)+\sin^2\theta_b W_2(k_z,\lambda,\tilde{\varphi})}{B(k_z,\lambda)}J_0(\lambda\tilde{\rho}) + \frac{\sin^2\theta_b W_3(k_z,\lambda,\tilde{\varphi})+\sin\theta_b\cos\theta_b W_4(k_z,\lambda,\tilde{\varphi})}{B(k_z,\lambda)}J_1(\lambda\tilde{\rho})\right] \times \lambda d\lambda \tag{19}$$

Assume that the feeding gap is sufficiently small, then the boundary condition requires that E_t approximately equals to $-V_0$ at the driving point and must be zero elsewhere on the surface of the tube. Thus, we have

$$E_t(r) = -V_0\delta(r) \tag{20}$$

where $\delta(r)$ denotes the Dirac delta function.

By combining (18) and (20), the boundary condition satisfied by the antenna should be

$$\frac{-i\omega\mu_0}{(2\pi)^2}\int_{-h}^{h}\int_0^{2\pi} G(\tilde{\rho},\tilde{\varphi},\tilde{z})\, I(r')d\theta' dr' = -V_0\delta(r) \tag{21}$$

C. DETERMINATION OF THE CURRENT DISTRIBUTION

It is known that the current distribution for a bare tubular antenna in a homogeneous isotropic medium has been examined and rigorously verified by King *et al.* [25]. Their proposed formula consisted of three trigonometric current terms, where the three indeterminate coefficients were evaluated through numerical methods. Based on King's theory, if we adopt similar procedures and take into account both the O-wave and E-wave in an anisotropic ionosphere, it then yields that the current distribution on a VLF space-borne tubular antenna could be expressed in the following form

$$I(r') = I_v^{(o)}\left[\sin k_o\left(h-|r'|\right) + T_u^{(o)}\left(\cos k_o r' - \cos k_o h\right) + T_d^{(o)}\left(\cos\frac{k_o r'}{2} - \cos\frac{k_o h}{2}\right)\right] + I_v^{(e)}\left[\sin k_e\left(h-|r'|\right) + T_u^{(e)}\left(\cos k_e r' - \cos k_e h\right) + T_d^{(e)}\left(\cos\frac{k_e r'}{2} - \cos\frac{k_e h}{2}\right)\right] \tag{22}$$

where $I_v^{(o)}$, $T_u^{(o)}$, $T_d^{(o)}$, $I_v^{(e)}$, $T_u^{(e)}$, and $T_d^{(e)}$ denote the complex amplitude coefficients for the O-wave and E-wave, respectively, they are yet to be determined. Besides, k_o and k_e represent the wave numbers for the O-wave and E-wave when the propagation direction is oriented along the antenna, they are also functions of θ_b. We write

$$k_{o,e}^2(\theta_b) = \frac{k_0^2}{2\left(\varepsilon_1\sin^2\theta_b+\varepsilon_3\cos^2\theta_b\right)}\left[\varepsilon_1\varepsilon_3\left(1+\cos^2\theta_b\right) \pm\sqrt{\left(\varepsilon_1^2-\varepsilon_2^2-\varepsilon_1\varepsilon_3\right)^2\sin^4\theta_b + 4\varepsilon_2^2\varepsilon_3^2\cos^2\theta_b} + \left(\varepsilon_1^2-\varepsilon_2^2\right)\sin^2\theta_b\right] \tag{23}$$

Next, we will solve the six indeterminate coefficients via the method of moments (MoM) [29]. By letting

$$I_1(r') = \sin k_o\left(h-|r'|\right) \tag{24}$$
$$I_2(r') = \cos k_o r' - \cos k_o h \tag{25}$$
$$I_3(r') = \cos\frac{k_o r'}{2} - \cos\frac{k_o h}{2} \tag{26}$$
$$I_4(r') = \sin k_e\left(h-|r'|\right) \tag{27}$$
$$I_5(r') = \cos k_e r' - \cos k_e h \tag{28}$$
$$I_6(r') = \cos\frac{k_e r'}{2} - \cos\frac{k_e h}{2} \tag{29}$$

and

$$V_j(r) = \int_{-h}^{h}\int_0^{2\pi} G(\tilde{\rho},\tilde{\varphi},\tilde{z})\, I_j(r')d\theta' dr' \tag{30}$$

where $j = 1, 2, 3, 4, 5, 6$, (22) can be rewritten as

$$I(r') = I_v^{(o)}\left[I_1(r') + T_u^{(o)}I_2(r') + T_d^{(o)}I_3(r')\right] + I_v^{(e)}\left[I_4(r') + T_u^{(e)}I_5(r') + T_d^{(e)}I_6(r')\right] \tag{31}$$

Also, (18) can be rewritten as

$$E_t(r) = \frac{-i\omega\mu_0}{(2\pi)^2}\left\{I_v^{(o)}\left[V_1(r) + T_u^{(o)}V_2(r) + T_d^{(o)}V_3(r)\right] + I_v^{(e)}\left[V_4(r) + T_u^{(e)}V_5(r) + T_d^{(e)}V_6(r)\right]\right\} \quad (32)$$

Now we multiply a function $I_i(r)$ on both sides of (32) and make an integration to r between $-h$ and h. When repeating this step for all I_1–I_6, the above equation could be reformulated in terms of matrix multiplication. By further using the boundary condition (20) and rearrangements, (32) becomes

$$V_0 \cdot \tilde{I} = \frac{i\omega\mu_0}{(2\pi)^2}\left(\tilde{M} \cdot \tilde{C}\right) \quad (33)$$

where

$$\tilde{I} = [I_1(0) \quad I_2(0) \quad I_3(0) \quad I_4(0) \quad I_5(0) \quad I_6(0)]' \quad (34)$$

$$\tilde{C} = \left[I_v^{(o)} \; I_v^{(o)}T_u^{(o)} \; I_v^{(o)}T_d^{(o)} \; I_v^{(e)} \; I_v^{(e)}T_u^{(e)} \; I_v^{(e)}T_d^{(e)}\right]' \quad (35)$$

The superscript $'$ in above vectors denotes matrix transpose, and $\tilde{M}$ is a 6×6 matrix with each of its component expressed as follows

$$M_{ij} = \int_{-h}^{h} I_i(r)V_j(r)dr = \int_{-h}^{h}\int_{-h}^{h}\int_{0}^{2\pi} G(\tilde{\rho}, \tilde{\varphi}, \tilde{z})\, I_i(r')I_j(r)d\theta' dr' dr \quad (36)$$

Considering that $\tilde{\rho}$, $\tilde{\varphi}$, $\tilde{z}$ are also functions of θ', r', r, $G(\tilde{\rho}, \tilde{\varphi}, \tilde{z})$ can be replaced by $G(\theta', r', r)$ and the final formula for M_{ij} is

$$M_{ij} = \int_{-h}^{h}\int_{-h}^{h}\int_{0}^{2\pi} G(\theta', r', r)I_i(r')I_j(r)d\theta' dr' dr \quad (37)$$

where $i, j = 1, 2, 3, 4, 5, 6$.

It is worth mentioning that the kernel function $G(\theta', r', r)$ in above equation contains a double infinite integral, which can be precisely evaluated through the method for computing the near-field [23]. However, there still exists a triple finite integral in each element of $\tilde{M}$. Thus in the next section, we will address the evaluating method for this triple integral.

D. EVALUATION OF MATRIX $\tilde{M}$

Here, we adopt a Gauss-Legendre quadrature (GLQ) [30] to process the triple integral in M_{ij}. The basic idea for the GLQ can be described by the following equation

$$\int_{-1}^{1} f(x)dx \approx \sum_{i=0}^{n} w_i f(x_i) \quad (38)$$

where x_i are zeros of the Legendre polynomials, and w_i are the corresponding Gauss coefficients.

With the help of linear transformation, a finite integral between the interval $[X_1, X_2]$ could be approximated as

$$\int_{X_1}^{X_2} f(x)dx = \frac{X_2 - X_1}{2}\int_{-1}^{1} f\left(\frac{X_2 - X_1}{2}x + \frac{X_1 + X_2}{2}\right)dx \approx \frac{X_2 - X_1}{2}\sum_{i=0}^{n} w_i f\left(\frac{X_2 - X_1}{2}x_i + \frac{X_1 + X_2}{2}\right) \quad (39)$$

If we let

$$w_i' = \frac{X_2 - X_1}{2}w_i, \quad x_i' = \frac{X_2 - X_1}{2}x_i + \frac{X_1 + X_2}{2} \quad (40)$$

then (39) becomes

$$\int_{X_1}^{X_2} f(x)dx = w_i'\sum_{i=0}^{n} f(x_i') \quad (41)$$

By applying the above method to (37) in an iterative way, the integral of M_{ij} can be converted to a triple sum form. We write

$$M_{ij} = \sum_{i=0}^{n} w_i'\left\{\sum_{j=0}^{m} w_j'\left[\sum_{p=0}^{q} w_p' f(\theta_i', r_j', r_p)\right]\right\} \quad (42)$$

where

$$f(\theta_i', r_j', r_p) = G(\theta_i', r_j', r_p)I(r_j')I(r_p) \quad (43)$$

Once every component of $\tilde{M}$ is calculated, the current distribution on the antenna can be completely determined by solving the six indeterminate coefficients in vector $\tilde{C}$. Moreover, the input impedance of the antenna Z_{in} is also obtained readily. We have

$$Z_{in} = \frac{V_0}{I(0)} \quad (44)$$

By now, we have provided the complete procedures for evaluating the current distribution and input impedance of a VLF space-borne tubular antenna. Next, we will carry out the corresponding computations and analyses.

III. COMPUTATIONS AND DISCUSSIONS

Since the O-wave is a fast attenuating wave while the E-wave is the propagable one, we will choose the phase constant of the E-wave, i.e., $\beta_e = \mathrm{Re}(k_e)$, as the reference quantity. By using the aforementioned method, the six indeterminate coefficients in the current distribution are computed with different antenna radii and the results are listed in Table 1. The parameters are taken as follows: the operating frequency is $f = 12.5$ kHz, the drive voltage is $V_0 = 1$ V, the half length of the antenna is $h = 50$ m, the magnitude of the earth's magnetic field is $B_0 = 0.5 \times 10^{-4}$ T, and the electron density and collision frequency of the ionosphere are taken as $N = 1.4 \times 10^{12}$ m^{-3}, $\nu = 10^3$ s^{-1}, respectively. Then we have $\omega_0 = 6.6 \times 10^7$ arc/s, $\omega_H = 8.6 \times 10^6$ arc/s, and the relation $\omega < \omega_H < \omega_0$ is satisfied. Here, we firstly discuss the most general case, i.e. let $\theta_b = 0°$. It is found that the amplitudes of $I_v^{(o)}$ and $I_v^{(e)}$ will increase with the radius of the antenna, whereas the rest four coefficients are decreased when the radius becomes larger. As is different with that of a space-borne linear antenna, the coefficients for the O-wave and E-wave have very similar amplitudes when assuming the currents concentrating on the antenna surface. Nevertheless, considering the O-wave is an evanescent wave, it is still necessary to raise the coefficients for the E-wave as high as possible while diminish the coefficients for the O-wave.

TABLE 1. Amplitude coefficients for the O-wave and E-wave of a VLF space-borne tubular antenna with different radii.

a (m)	0.001	0.003	0.005	0.01	0.015	0.02
$\mathrm{Re}I_v^{(o)}$	-3.791×10^{-5}	1.523×10^{-2}	8.675×10^{-1}	-1.039×10^{1}	-6.245×10^{0}	2.476×10^{0}
$\mathrm{Im}I_v^{(o)}$	3.534×10^{-5}	3.611×10^{-1}	3.241×10^{0}	5.355×10^{-1}	3.892×10^{1}	6.885×10^{1}
$\mathrm{Re}T_u^{(o)}$	-4.766×10^{4}	4.100×10^{0}	2.824×10^{1}	-3.144×10^{2}	-5.534×10^{1}	5.104×10^{0}
$\mathrm{Im}T_u^{(o)}$	-4.184×10^{4}	1.486×10^{2}	2.749×10^{2}	3.932×10^{2}	1.236×10^{2}	9.638×10^{0}
$\mathrm{Re}T_d^{(o)}$	7.832×10^{5}	-6.772×10^{1}	-4.647×10^{2}	5.164×10^{3}	9.089×10^{2}	-8.389×10^{1}
$\mathrm{Im}T_d^{(o)}$	6.872×10^{5}	-2.619×10^{3}	-4.694×10^{3}	-6.639×10^{3}	-2.208×10^{3}	-3.366×10^{2}
$\mathrm{Re}I_v^{(e)}$	-1.560×10^{-4}	1.103×10^{0}	9.932×10^{0}	1.386×10^{0}	1.188×10^{2}	2.096×10^{2}
$\mathrm{Im}I_v^{(e)}$	1.233×10^{-4}	-4.673×10^{-2}	-2.667×10^{0}	3.195×10^{1}	1.923×10^{1}	-7.576×10^{0}
$\mathrm{Re}T_u^{(e)}$	-1.402×10^{4}	-6.434×10^{1}	-1.076×10^{2}	-1.489×10^{2}	-5.577×10^{1}	-1.638×10^{1}
$\mathrm{Im}T_u^{(e)}$	-1.039×10^{4}	1.442×10^{0}	9.705×10^{0}	-1.067×10^{2}	-1.903×10^{1}	1.774×10^{0}
$\mathrm{Re}T_d^{(e)}$	2.180×10^{5}	9.037×10^{2}	1.577×10^{3}	2.219×10^{3}	7.702×10^{2}	1.574×10^{2}
$\mathrm{Im}T_d^{(e)}$	1.617×10^{5}	-2.230×10^{1}	-1.508×10^{2}	1.660×10^{3}	2.963×10^{2}	-2.757×10^{1}

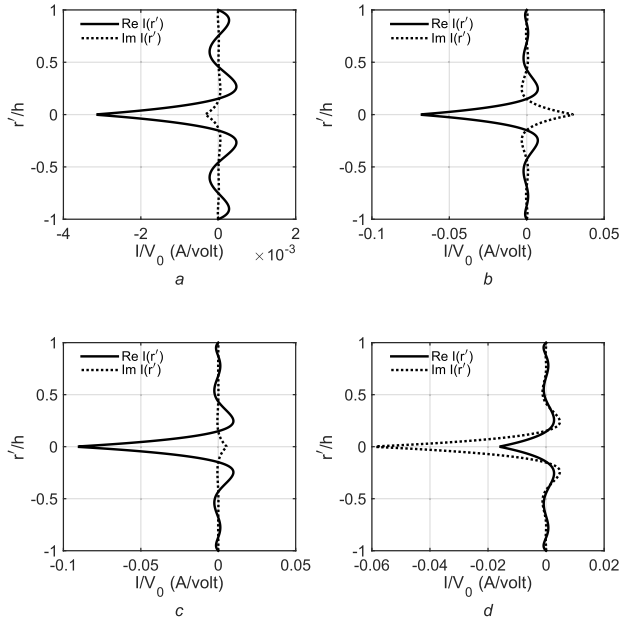

FIGURE 2. Current distributions on a VLF space-borne tubular antenna at (a) $\beta_e h = 0.211$, (b) $\beta_e h = 0.423$, (c) $\beta_e h = 0.845$, (d) $\beta_e h = 1.056$.

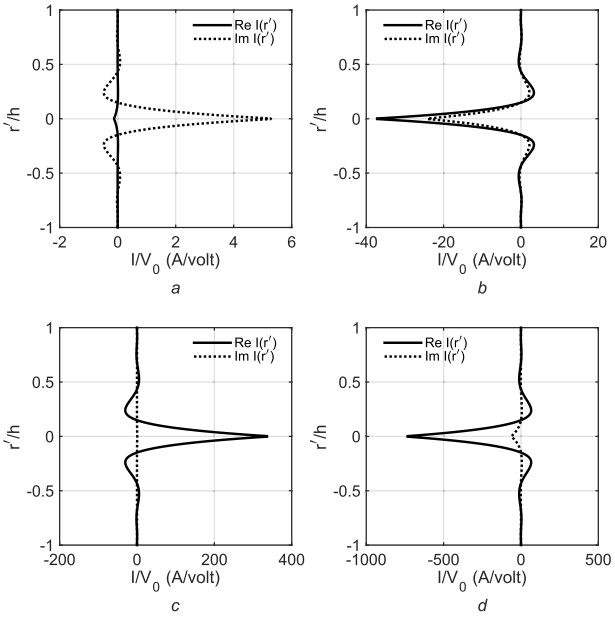

FIGURE 3. Current distributions on a VLF space-borne tubular antenna at (a) $\beta_e h = 1.584$, (b) $\beta_e h = 2.007$, (c) $\beta_e h = 2.641$, (d) $\beta_e h = 2.958$.

After obtaining the amplitude coefficients, the normalized current distributions at different electrical lengths ($\beta_e h$) of a VLF space-borne tubular antenna are shown in Figs. 2 and 3. The radius of the antenna is taken as $a = 0.01$ m, and all other parameters are same with those used in Table 1. It is found that due to the complex characteristics of the ionosphere in the VLF range, the distributions for both the real and imaginary currents on the antenna are not fixed, but will change significantly with the electrical length of the antenna. We may observe that when the electrical length of the antenna is small (say $\beta_e h < 1$), the amplitude of the current does not exhibit remarkable regularity. However, once the electrical length exceeds a certain value (in this case, $\beta_e h \geq 1$), the magnitude of the current will increase with the electrical length of the antenna monotonically. This is probably because for antennas with small lengths, their sizes are more comparable to the wavelength and the current magnitude is thereby more susceptible to the electrical length of the antenna. Meanwhile, the symmetric current distribution always reaches its maximum at the driving point, and will gradually tends to zero at the two terminals (i.e. close to triangular distributions). This indicates that the main contribution of the radiation comes from the central part of the antenna, and how to increase the total current moment on the antenna with limited power will be the key to improve the antenna efficiency. To the best of our knowledge, the real part of the current represents the active power while the imaginary part represents the reactive power, and the latter is the power loss. Thus, in order to improve the efficiency, the electrical length should be adjusted properly so as to make the imaginary current as small as possible.

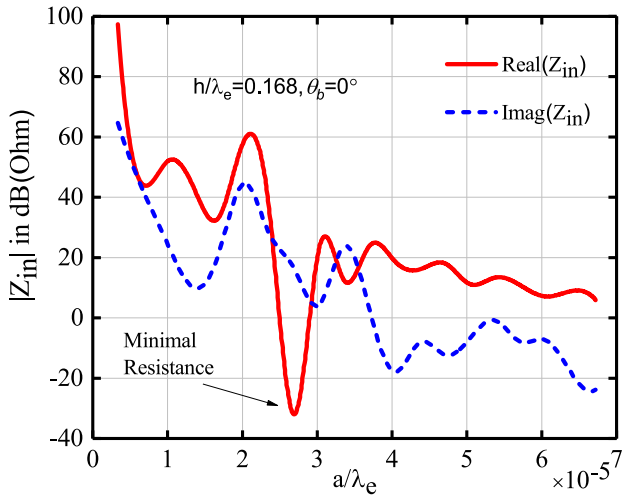

FIGURE 4. Input impedance of a VLF space-borne tubular antenna versus antenna radius.

With the current distribution determined, the input impedance of the antenna is also computed under several different conditions. Fig. 4 shows the results for the input impedance varying with the dimensionless variable a/λ_e (where $\lambda_e = 2\pi/\beta_e$ denotes the wavelength of the E-wave). The half length of the antenna in Fig. 4 is taken as $h = 50$ m and all other parameters remain constant. It is seen that because of the complex anisotropic properties of the ionosphere at the VLF range, the input impedance of a VLF space-borne tubular antenna does not vary monotonously, but will decrease with evident fluctuations as the radius increases. As a whole, both the real and imaginary parts of the input impedance are smaller when the radius becomes larger, indicating that the overall efficiency of the antenna is increasing with the antenna radius. Despite that, pronounced minima can still be observed at certain points. It means that once the radius is restricted to a certain range, there exists an optimal value. What's more, in the real air and space environment, even if the input impedance will always decrease with the increase of the radius, the radius of the antenna is limited and it is impossible to make the radius infinitely large. This somewhat arbitrary radius must be thick enough so as not to burn out when the current is large, but thin enough to avoid too heavy to launch. In the meanwhile, in practical engineering applications, manufacturing cost is also another significant factor that needs to be carefully considered. Since in most cases, thicker antenna means higher cost.

Also of interest is the relationship between variations of the input impedance and the electrical length. Both the tubular and linear antenna model are considered and depicted in Fig. 5. All the parameters are still the same as those in former figures except $\theta_b = 30°$ in Fig. 5a and $\theta_b = 60°$ in Fig. 5b, respectively. By observing the tubular curves, similar with Fig. 4, the input impedance will also show an overall downward trend with the increase of the electrical length and pronounced minima can still be observed. Considering enlarging the length of the antenna will also

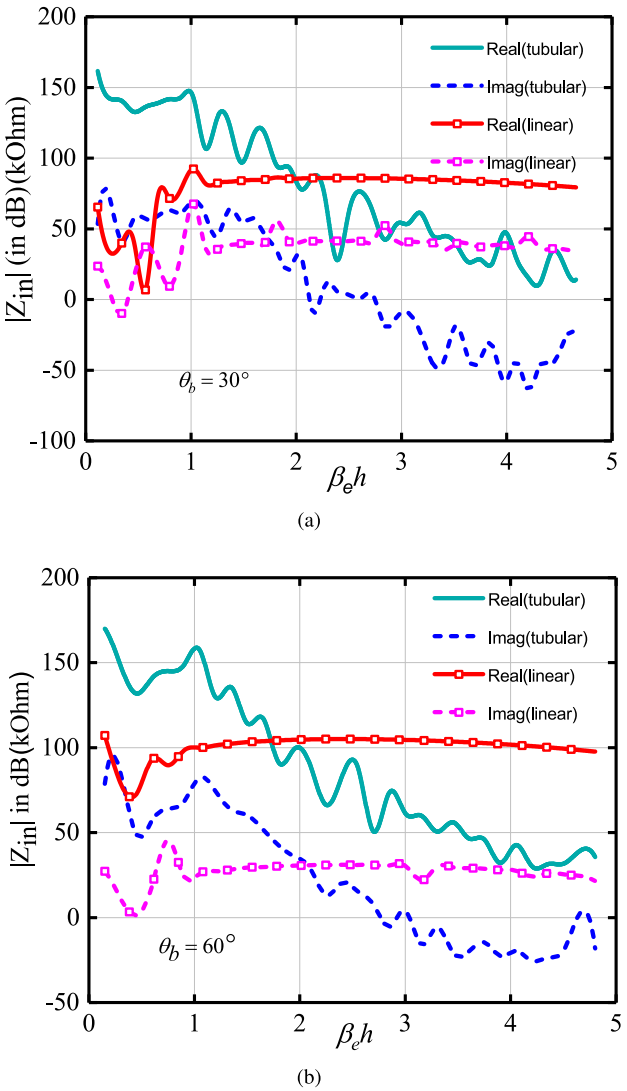

FIGURE 5. Input impedance of VLF space-borne tubular and linear antennas versus electrical length of the antenna. (a) $\theta_b = 30°$, (b) $\theta_b = 60°$.

inevitably augment the manufacturing costs, it is more desirable to decrease the antenna impedance by selecting proper parameters. From a comparison of curves labeled tubular and linear in Fig. 5, it is noted that when the electrical length is relatively small, the input impedance of these two models has similar trends. With the further increase of the length, there is very little change of the linear one, whereas the tubular one will continue decline. Hence the difference between these two models lead to the following conclusion, the input impedance of a tubular antenna is somewhat smaller than that of a linear antenna once the electrical length is sufficiently large.

It is known that in the VLF range the electron collision frequency ν is much greater than the angular frequency ω, which is the main reason for the strong anisotropy of the ionosphere. However, as ω increases, the contribution of ν to the relative dielectric tensor $\hat{\varepsilon}$ becomes smaller, and even can be neglected at last. Under this circumstance, the ionosphere can be considered transparent for high-frequency

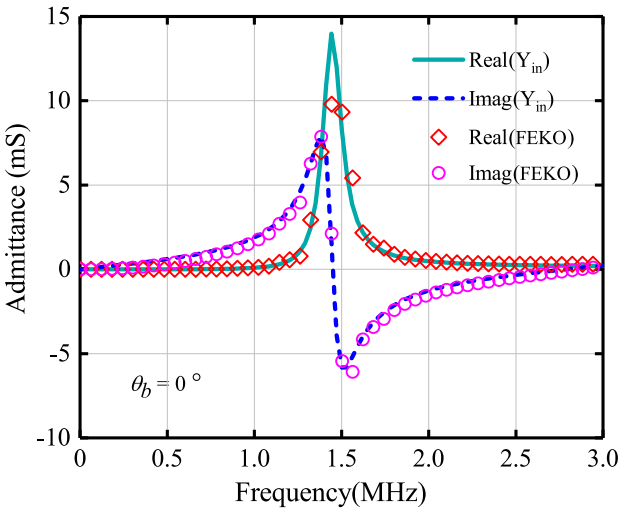

FIGURE 6. Comparison with FEKO results versus frequency.

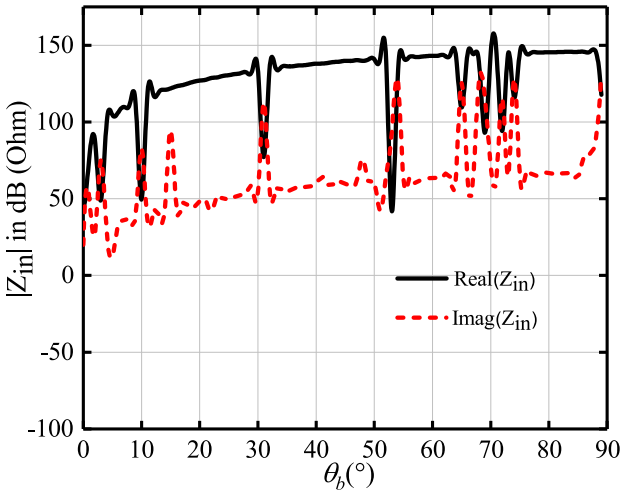

FIGURE 7. Input impedance of a VLF space-borne tubular antenna versus the geomagnetic inclination angle.

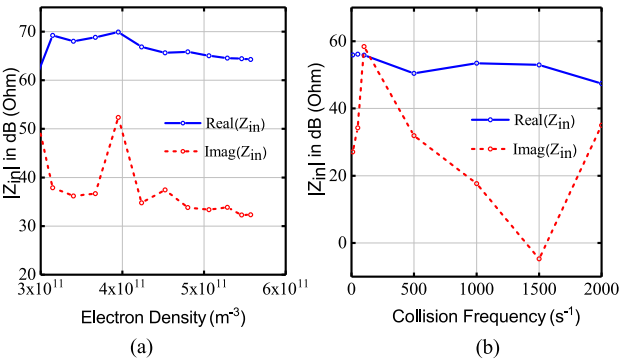

FIGURE 8. Input impedance of VLF space-borne tubular versus some environmental changes. (a) electron density, (b) collision frequency.

electromagnetic waves, in other words, as if they were in free space. Therefore attention will be restricted to MHz frequencies and comparisons are made with numerical solutions taken from FEKO in Fig. 6. Here the radius and length of the antenna are $a = 0.01$ m and $2h = 100$ m, while all parameters of the ionosphere are still the same as those used in Table 1. Apparently, the analytical curve and FEKO curve variation tendencies were approximate and unanimous, completely confirming the high accuracy of our method. It can also be seen that, with increasing frequency, the value of the input admittance increases first and then decreases, reaching a maximum near $f = 1.5$ MHz. In this case, the wavelength is 200 m and the length of the antenna is 100 m. It means the result shows a great correspondence with the well-known theory that half-wavelength antenna has the smallest input impedance and is highly efficient in an isotropic medium.

As pointed out by Li and Pan [31], only when $\tan^2\theta < -\varepsilon_3/\varepsilon_1$, the E-wave can be a propagable one. Therefore, the critical angle θ_A in the VLF range can be obtained in the form of $\theta_A = \arctan\sqrt{-\varepsilon_3/\varepsilon_1} \approx 89°$. To further explore the effect of the geomagnetic inclination angle to the antenna, Fig. 7 shows the input impedance of the antenna over the angle θ_b from 0° to 89° for fixed $h = 1$ m and $a = 0.001$ m. The angular frequency is $f = 12.5$ kHz. It is found that the input impedance will also show a rising trend with obvious fluctuations as θ_b varies, illustrating that the impedance of a VLF space-borne tubular antenna is very sensitive to its relative posture to the background magnetic field. It is also noteworthy that though there exist some sudden dips of the real part in certain angles like around 50°, meanwhile the imaginary one is somewhat large. Considering all of the above, we may infer that overall, the optimal orientation for a VLF space-borne tubular antenna shoule be as parallel as possible to the earth's magnetic field since the antenna has a smaller input impedance when θ_b approaches to 0°. However, if all other parameters are fixed, it is possible to find other optimal angles.

According to the data given by [32], the electron density will exhibit totally different characteristics at different heights. Since we are considering low-Earth orbit satellites of 300–400 kilometers high, simulation to show its impact to the final input impedance in this range is made and the result is depicted in Fig. 8a. It is seen that if it increases, the input impedance will decrease slowly in general but the change is not large. Maybe it is because within 300–400 km, the change of the electron density N is relatively very little. Compared with the order of magnitude of N, its effect on the final result is limited. The discussion of the impact of the collision frequency comes next in Fig. 8b. As the collision frequency increases, the real part of the input impedance does not change drastically, whereas the imaginary one will fluctuate violently. We speculate the reason maybe that the variation in collision frequency directly affects some components of the relative dielectric tensor. Changes in the dielectric tensor, in turn, will have a direct effect on the entire integrand. Therefore, the effect of a certain variable on the final input impedance is very complicated, not a single positive or negative correlation. And further work is required to draw a more specific conclusion. In fact, the environmental changes like altitude, temperature, electron concentration, day-night changes, alternating seasons, and even solar activity can cause

changes of the ionosphere, but all of them are reflected through the dielectric tensor $\hat{\varepsilon}$ in our problem. Therefore, no matter how the environment changes, our method of evaluating the antenna always works.

IV. CONCLUSION

In this paper, we treat the problem of a VLF tubular antenna in an anisotropic cold plasma both analytically and numerically, and propose a theoretical method for computing the current distribution and input impedance of the antenna. The assumed current distribution includes the effects of both the O-wave and E-wave and thereby has a more complicated form. The kernel function of the antenna is also obtained by evaluating the near-field, and the six amplitude coefficients in the current equation are determined through the MoM as well as the GLQ algorithm. Computations reveal that the current distribution and input impedance of a VLF space-borne tubular antenna are quite sensitive to parameter changes and may vary unpredictably. Overall, the efficiency of the antenna will to some extent be improved as the radius or electrical length of the antenna increases. However, for economic purpose, the dimension of the antenna should be selected appropriately so that the antenna can possess a larger current moment and a smaller input impedance with its size limited. To demonstrate the accuracy of the proposed method, comparisons with the linear antenna model and numerical solutions simulated in FEKO are also carried out subsequently. Moreover, we find that the antenna has a smallest input impedance when θ_b is close to 0° with several sudden dips in some certain angles. Hence in practical applications the orientation of the antenna should be as parallel as possible to the direction of the geomagnetic field in order to achieve maximum efficiency. But for a specific set of antenna parameters, perhaps one can find more than one optimal inclination angles. Qualitative discussions of environmental changes are also presented in the end. In summary, by determining the optimal antenna parameters in a variable ionospheric environment, the proposed method may provide heuristic advice to the design of a practical VLF space-borne tubular antenna.

REFERENCES

[1] K. Rawer, D. Bilitza, and S. Ramakrishnan, "Goals and status of the international reference ionosphere," *Rev. Geophys.*, vol. 16, pp. 177–181, May 1978.

[2] R. A. Helliwell, *Whistlers and Related Ionospheric Phenomena*, 2nd ed. Mineola, NY, USA: Dover, 2006, pp. 23–24.

[3] J. A. Carroll, "The small expendable deployment system (SEDS)," in *Proc. 2nd Int. Conf. Space Tethers Sci. Space Station Era.*, Venice, Italy, Oct. 1987, pp. 43–50.

[4] N. A. Armand, I. P. Semenov, B. E. Chertok, V. V. Migulin, and V. V. Akindinov, "Experimental investigation of the VLF radiation of a loop antenna installed on the Mir-progress-28-Soyuz TM-2 orbital complex in the earth's ionosphere," (in Russian), *Radiotekhnika Elektronika*, vol. 33, pp. 2225–2233, Nov. 1988.

[5] R. Deloach, J. Diamond, T. Finley, and R. Rhew, "End-mass instrumentation for the first SEDS/Delta II mission," in *Proc. 28th Aerosp. Sci. Meeting*, Jan. 1990, p. 537.

[6] P. R. Bannister, J. K. Harrison, C. C. Rupp, R. W. P. King, M. L. Cosmo, E. C. Lorenzini, C. J. Dyer, and M. D. Grossi, "Orbiting transmitter and antenna for spaceborne communications at ELF/VLF to submerged submarines," in *Proc. AGARD, ELF/VLF/LF Radio Propag. Syst. Aspects*, vol. 529, May 1993, pp. 1–14.

[7] V. A. Koshelev and V. M. Melnikov, *Large Space Structures Formed by Centrifugal Forces*. Boca Raton, FL, USA: CRC Press, 1998.

[8] TSS. *NASA Science Missions*. Accessed: Aug. 1, 2019. [Online]. Available: http://science.nasa.gov/missions/tss/

[9] IMAGE. *NASA Science Missions*. Accessed: Jun. 4, 2020. [Online]. Available: https://science.nasa.gov/missions/image.

[10] Space Tethers. *Satellite Missions*. Accessed: Jun. 10, 2020. [Online]. Available: https://earth.esa.int/web/eoportal/satellite-missions/s/space-tethers

[11] *Zhangheng-1(CSES)*. Accessed: May 31, 2020. [Online]. Available: https://spacelaunchnow.me/launch/long-march-2d-zhangheng-1-cses/

[12] P. Nikitin and C. Swenson, "Impedance of a short dipole antenna in a cold plasma," *IEEE Trans. Antennas Propag.*, vol. 49, no. 10, pp. 1377–1381, Oct. 2001.

[13] T. F. Bell, U. S. Inan, and T. Chevalier, "Current distribution of a VLF electric dipole antenna in the plasmasphere," *Radio Sci.*, vol. 41, no. 2, pp. 1–14, Apr. 2006.

[14] T. W. Chevalier, U. S. Inan, and T. F. Bell, "Terminal impedance and antenna current distribution of a VLF electric dipole in the inner magnetosphere," *IEEE Trans. Antennas Propag.*, vol. 56, no. 8, pp. 2454–2468, Aug. 2008.

[15] T. M. Zaboronkova, A. V. Kudrin, and E. Y. Petrov, "VHF current distribution on a cylindrical VLF antenna in a magnetoplasma," *Radiophysics Quantum Electron.*, vol. 42, no. 8, pp. 660–673, Aug. 1999.

[16] A. V. Kudrin, E. Y. Petrov, and T. M. Zaboronkova, "Current distribution and input impedance of a loop antenna in a cold magnetoplasma," *J. . Waves Appl.*, vol. 15, no. 3, pp. 345–378, Jan. 2001.

[17] A. V. Kudrin, A. S. Zaitseva, T. M. Zaboronkova, and S. S. Zilitinkevich, "Current distribution and input impedance of a strip loop antenna located on the surface of a circular column filled with a resonant magnetoplasma," *Prog. Electromagn. Res. B*, vol. 55, pp. 241–256, 2013.

[18] Y. V. Chugunov, E. A. Shirokov, and I. A. Fomina, "On the theory of a short cylindrical antenna in anisotropic media," *Radiophys. Quantum Electron.*, vol. 58, no. 5, pp. 318–326, Oct. 2015.

[19] K. Li, X. Y. Sun, and H. T. Zhai, "Propagation of ELF electromagnetic waves in the lower ionosphere," *IEEE Trans. Antennas Propag.*, vol. 59, no. 2, pp. 661–666, Feb. 2011.

[20] W. Y. Pan, and K. Li, *Propagation of SLF/ELF Electromagnetic Waves*. Berlin, Germany: Springer-Verlag, 2014, ch. 7.

[21] T. He, X. W. Zhang, W. Y. Pan, and K. Li, "Current distribution and input impedance of a VLF linear antenna in an anisotropic plasma," *IEEE Trans. Antennas Propag.*, vol. 67, no. 3, pp. 1519–1526, Mar. 2019.

[22] T. He, H. R. Zeng, and K. Li, "VLF current distribution and input impedance of an arbitrarily oriented linear antenna in a cold plasma," *IEEE Access*, vol. 7, pp. 80861–80869, Jul. 2019.

[23] T. He, X. W. Zhang, W. Y. Pan, and K. Li, "Near-field of a VLF electric dipole in an anisotropic plasma," *IEEE Trans. Antennas Propag.*, vol. 67, no. 6, pp. 4040–4048, Jun. 2019.

[24] D. Chang and J. Wait, "Theory of a vertical tubular antenna located above a conducting half-space," *IEEE Trans. Antennas Propag.*, vol. AP-18, no. 2, pp. 182–188, Mar. 1970.

[25] R. W. P. King, G. S. Smith, M. Owens, and T. T. Wu, *Antennas in Matter—Fundamentals, Theory, and Applications*. Cambridge, MA, USA: MIT Press, 1981, ch. 7.

[26] H. Shen and T. T. Wu, "The universal current distribution near the end of a tubular antenna," *J. Math. Phys.*, vol. 30, no. 11, pp. 2721–2729, Nov. 1989.

[27] B. Bhat, "Current distribution on an infinite tubular antenna immersed in a cold collisional magnetoplasma," *Radio Sci.*, vol. 8, no. 5, pp. 483–492, May 1973.

[28] K. G. Budden, *Radio waves in the Ionosphere*. Cambridge, UK: Cambridge Univ. Press, vol. 1961, ch. 3.

[29] M. N. O. Sadiku, *Numerical Techniques in Electromagnetics*, 2nd ed., NY, USA: CRC Press, 2001, ch. 5.

[30] M. Abramowitz, and I. A. Stegun, Eds. "Handbook of mathematical functions with formulas, graphs, and mathematical tables," in *Applied Mathematics Series*, 1st ed. New York, NY, USA: Dover, 1972, ch. 25.4.

[31] K. Li and W. Y. Pan, "Radiation of an electric dipole in an anistropic medium," *Indian J. Radio Spave Phys.*, vol. 26, Dec. 1997, Art. no. 340345.

[32] *International Reference Ionosphere–IRI (2016) With IGRF–13 Coefficients*. Accessed: Jun. 15, 2020. [Online]. Available: https://ccmc.gsfc.nasa.gov/modelweb/models/iri2016_vitmo.php

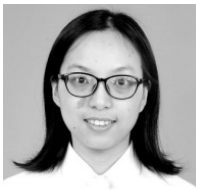

LINA HE (Graduate Student Member, IEEE) was born in Shaoxing, Zhejiang, China, in July 1992. She received the B.S. degree from the Zhejiang University of Technology (ZJUT), Hangzhou, Zhejiang, China, in 2014. She is currently pursuing the Ph.D. degree in electronic science and technology with the College of Information Science and Electronic Engineering, Zhejiang University, Hangzhou.

Her current research interest includes radio wave propagation theory and its applications.

TONG HE (Member, IEEE) was born in Hangzhou, Zhejiang, China, in 1990. He received the B.S. degree in electrical engineering and automation from the University of Electronic Science and Technology of China (UESTC), Chengdu, China, in 2013, the M.S. degree in electrical engineering from the University of Michigan-Dearborn, Dearborn, MI, USA, in 2014, and the Ph.D. degree in electronic science and technology from Zhejiang University, Hangzhou, China, in 2019.

Since July 2019, he has been an Associate Researcher with the Intelligent Network Center, Zhejiang Lab, Hangzhou. His current research interests include electromagnetic wave propagation and antenna theory.

HUI RAN ZENG (Graduate Student Member, IEEE) was born in Chongqing, China, in November 1995. She received the B.S. degree in electronic and information engineering from the East China University of Science and Technology, Shanghai, China, in 2017. She is currently pursuing the Ph.D. degree in electromagnetic field and microwave technology with the College of Information Science and Electronic Engineering, Zhejiang University, Hangzhou, Zhejiang, China.

Her current research interests include electromagnetic wave propagation and antenna theory.

KAI LI was born in Xiao County, Anhui, China, in February 1968. He received the B.S. degree in physics from Fuyang Normal University, Anhui, in 1990, the M.S. degree in radio physics from Xidian University, Xi'an, China, in 1994, and the Ph.D. degree in astrophysics from the Shaanxi Astronomical Observatory, Chinese Academy of Sciences, Shaanxi, China, in 1998.

From August 1990 to December 2000, he was on the faculty of the China Research Institute of Radiowave Propagation (CRIRP). From January 2001 to December 2002, he was a Postdoctoral Fellow with Information and Communications University (ICU), Daejeon, South Korea. From January 2003 to January 2005, he was a Research Fellow with the School of Electrical and Electric Engineering, Nanyang Technological University (NTU), Singapore. Since January 2005, he has been a Professor with the College of Information Science and Electronic Engineering, Zhejiang University, Hangzhou, China. His current research interests include classical electromagnetic theory and radio wave propagation.

Dr. Li is a Senior Member of the Chinese Institute of Electronics (CIE) and a member of the Chinese Institute of Space Science (CISS).